

To appear in *Astronomical Journal*

## **Globular Clusters around Galaxies in Groups**

Cristiano Da Rocha, Claudia Mendes de Oliveira

*Instituto de Astronomia, Geofísica e Ciências Atmosféricas, Universidade de São Paulo,  
Av. Miguel Stefano 4200, 04301-904, São Paulo – SP, Brazil*

Michael Bolte

*UCO/Lick Observatory, Department of Astronomy and Astrophysics,  
University of California, Santa Cruz, California 95064*

Bodo L. Ziegler

*Universitätssternwarte Göttingen, Geismarlandstr. 11, 37083 Göttingen, Germany*

and

Thomas H. Puzia

*Universitätssternwarte München, Scheinerstr. 1, D-81679 München, Germany*

**ABSTRACT**

We have obtained deep photometry of NGC 1199 (in the compact group HCG 22) and NGC 6868 (in the Telescopium loose group) with the Keck II and the VLT-I telescopes. Both galaxies are the optically brightest galaxy of their groups. NGC 1199 has two companion galaxies at a median projected distance of only 33 *kpc* and, based in its peculiar internal structure and large X-ray halo, NGC 6868 has been proposed to be a merger remnant.

Our analysis of *B* and *R* images uncovered a population of globular clusters around both galaxies, with total (and local) specific frequency  $S_N = 3.6 \pm 1.8$  ( $3.4 \pm 1.5$ ) for NGC 1199 and  $S_N = 1.8 \pm 1.1$  ( $0.8 \pm 0.4$ ) for NGC 6868. The radial profile of the globulars of NGC 1199 follows the light distribution of the galaxy and can be fitted by a power-law and a “core model” with a very steep slope ( $\alpha = 2.5 \pm 0.3$ ). In the case of NGC 6868, the profile of the globulars is well fitted by a power-law and a “core model” profile of slope  $1.4 \pm 0.3$  and is shallower than the galaxy light distribution. Maximum-likelihood fitting of two Gaussians to the globular cluster color distribution yields a high significance for multi-modality with peaks centered at  $(B - R)_0 = 1.13 \pm 0.04$  and  $1.42 \pm 0.04$  (NGC 1199) and  $(B - R)_0 = 1.12 \pm 0.07$  and  $1.42 \pm 0.07$  (NGC 6868).

NGC 1199 and NGC 6868 are good examples of galaxies where the group environment are likely to have affected their dynamical evolution. We find that for NGC 1199, the properties of the globular cluster system are similar to those for other systems around external elliptical galaxies located in less dense environments, but with a very steep radial profile. In the case of NGC 6868, we find a regular radial profile and color distribution and a comparatively low specific frequency for the globular cluster system of the galaxy.

*Subject headings:* galaxies: star clusters — galaxies: elliptical and lenticular, cD — galaxies: individual (NGC 1199, NGC 6868)

## 1. Introduction

Variations in the properties of extragalactic globular cluster systems (GCS) as a function of the environment of the host galaxy hold some of the keys to understanding the formation and evolution of GCS. Environment has been proposed as one of the important factors in setting the specific frequency  $S_N$  (number of clusters normalized by galaxy luminosity). Harris, in a review paper of 1991, pointed out that elliptical galaxies in small groups and sparse environments, have, on average, half the  $S_N$  of elliptical galaxies in the Virgo and Fornax clusters (excluding the central galaxies which have the well known extremely high specific frequencies). On the other hand Djorgovski and Santiago (1992) found an increase of the  $S_N$  with the host galaxy luminosity, what was confirmed by Zepf, Geisler and Ashman (1994) (see Ashman and Zepf 1998; Elmegreen 2000; Harris 2001, for detailed discussion on the subject). As the majority of the very bright galaxies are found in clusters and the faint ones are in groups and in the field, the environmental effect

on the  $S_N$  and its luminosity dependency are not easily disentangled. The effects of host-galaxy environment on other details of the GCS, the radial and color distributions is not well documented.

The main goal of this work is to characterize the GCS of two galaxies in small groups: NGC 1199, the central elliptical galaxy in the compact group HCG 22 and NGC 6868, a suspected merger remnant in the center of the Telescopium group. In particular, we are looking for suggestions that the basic properties of the globular cluster systems around these galaxies have been modified by the dense environment of the compact group or the merger event respectively.

The compact group HCG 22 contains three bright galaxies. This group was originally cataloged as a quintet of galaxies (Hickson 1982). However, Hickson *et al.* (1992) showed this to be a triplet at a mean redshift of 0.009 with a superimposed discordant pair at  $z = 0.0296$ . The group has a median velocity of  $2686 \text{ km s}^{-1}$  and a velocity dispersion of  $\sim 54 \text{ km s}^{-1}$ . Based on the surface brightness fluctuation method, Tonry *et al.* (2001) derive a distance modulus  $(m - M)_V = 32.6 \pm 0.3$  to NGC 1199, the dominant galaxy of the group, corresponding to  $33.1 \text{ Mpc}$  and a median projected galaxy separation in the group of  $33 \text{ kpc}$  (Tonry *et al.* 2001, assume  $H_0 = 74 \text{ km s}^{-1} \text{ Mpc}^{-1}$ ). NGC 1199 (also known as HCG 22A) is classified as E2 (Hickson 1982).

NGC 6868 is also classified as an E2 (de Vaucouleurs *et al.* 1991). The Telescopium group contains five bright galaxies with a median velocity of  $2601 \text{ km s}^{-1}$ , and a velocity dispersion of  $\sim 219 \text{ km s}^{-1}$ . Tonry *et al.* (2001) measure  $(m - M)_V = 32.1 \pm 0.2$  based on the surface brightness fluctuation method which corresponds to a distance of  $26.8 \text{ Mpc}$  and a median projected separation for group galaxies of  $209 \text{ kpc}$ . Although NGC 6868 is located in an environment that has a number density of bright galaxies lower than that of a typical compact group, the interest in studying the globular cluster system of this galaxy is that it is almost certainly a recent merger (Hansen, Jørgensen and Nørgaard-Nielsen 1991). NGC 6868 appears to be an ordinary elliptical galaxy from its global properties, but, in a detailed study, Hansen *et al.* (1991) showed that there is a system of dust features close to the NGC 6868 core and a disk of ionized gas within  $1 \text{ kpc}$  of its center indicating the presence of a young population of stars. The kinematics of the gas disk was studied by Plana *et al.* (1998), who found a flat rotation curve with a velocity amplitude of  $\pm 150 \text{ km s}^{-1}$ . The presence of the dust structure and the ionized gas suggest that NGC 6868 may have captured one or more gas-rich galaxies. In addition NGC 6868 has a halo of X-ray gas associated with it. Its X-ray and optical luminosities are in good agreement with the  $L_B - L_X$  relation proposed by Beuing *et al.* (1999) for early-type galaxies. The general properties of the two galaxies can be seen in table 1.

The paper is organized as follows. Section 2 describes the observations and data reduction. In §3 we show the results and §4 has our discussion.

## 2. Observations and Data Reduction

### 2.1. Observations

The images of HCG 22 were obtained with the Keck II telescope in June 1997 using the Low-Resolution-Imaging Spectrometer (LRIS, Oke *et al.* 1995). Images in  $B$  and  $R$  of total exposure times of 720 seconds ( $4 \times 180$ ) and 630 seconds ( $7 \times 90$ ) were obtained with an average seeing, on the combined images, of 0.77 and 0.74 arcsec respectively. The field size is  $5.7 \times 7.3$  arcmin and the pixel size is 0.215 arcsec. The NGC 6868 images were obtained with the ESO/VLT-I in October 1999 using the Focal Reducer/Low Dispersion Spectrograph 1 (FORS1). Images in  $B$  and  $R$  with total exposure times of 900 seconds ( $5 \times 180$ ) and 810 seconds ( $9 \times 90$ ) were obtained with average seeing values, on the combined images, of 0.76 and 0.73 arcsec respectively. The field size is  $6.4 \times 6.4$  arcmin and the pixel size is 0.2 arcsec. Images in  $B$  and  $R$  of similar depth to the ones taken for NGC 6868 were obtained centered on a position  $10'$  from the galaxy center. This was meant to be our control field for background subtraction. The log of observations is shown in Table 2.

### 2.2. Data Reduction

#### 2.2.1. Image Processing and Photometry

Using the IRAF<sup>1</sup> package (Image Reduction and Analysis Facility) we carried out the basic image reduction procedures (bias correction, flatfielding and image combining). We next used the tasks ELLIPSE and BMODEL of the STSDAS package to model and subtract the light from bright galaxies. We masked the very bright objects on the images and the central regions of the giant galaxies that could not be modeled by ELLIPSE. Subtraction of the sky level of the image was done using the SExtractor package (Source Extractor) Version 2.1.6 (Bertin and Arnouts 1996) with the output option `-BACKGROUND` and a meshsize of 64 pix. The combined images for NGC 1199 and NGC 6868 and the final masked and background-subtracted images are shown in figure 1.

The combined, masked and background-subtracted images were then used for detection and photometry of the faint objects, using SExtractor, with a Gaussian convolution mask of 3 pixels for the HCG 22 images and of 4 pixels for the NGC 6868 images. For photometry of the objects we used the MAG\_AUTO value, which is given by an adaptive aperture photometry routine, and gives the total magnitude of the detected objects. The adaptive aperture photometry routine is based on the Kron (1980)’s “first moment” algorithm (for more details on the photometry see Bertin and Arnouts 1996). Monte Carlo simulations were made to test the reliability of the MAG\_AUTO photometry (see following section) and a small correction was added to the photometry of each

---

<sup>1</sup>IRAF is distributed by the National Optical Astronomy Observatories, which is operated by the Association of Universities for Research in Astronomy, Inc., under cooperative agreement with the National Science Foundation.

detected object.

The final list of objects includes only the objects that were detected in both  $B$  and  $R$  bands. We discarded all the objects that were within 5 arcsec of the borders of the images and within 5 arcsec of masked regions.

At the distance of our groups, globular clusters are point-like sources. To select them, we have excluded the extended objects (dwarf and background galaxies) from our final list. Using the results from the add-star experiments (described in the next section) we could define the range of FWHM where we expect the point-like sources to be found, as a function of their magnitudes. The FWHM value is measured by SExtractor. Taking the average of the FWHM on the  $R$  band, in 0.5 magnitude bins, of the simulated objects and using a  $1\sigma$  rejection level, we could determine a “point-like source locus” on the magnitude–FWHM plane for each of the images. The detected objects located inside this region, along the magnitude range for each image, were classified as point-like sources and all the other objects were excluded from the final list. This method has shown, in our case, better results than the default SExtractor star–galaxy separations. The selection of point-like sources using the magnitude–FWHM plane was previously used to select GC candidates by Rhode and Zepf (2001). The magnitude–FWHM plots for our fields are shown in figure 2.

Calibration of the images of HCG 22 was done using images from the CTIO 1.5–meter telescope. We have calibrated those HCG 22 images in  $B$  and  $R$  bands using Landolt (1992) standard stars and then calibrated the Keck II images using the surface brightness profile of NGC 1199. The final RMS of these calibrations are 0.011 for the  $B$  band and 0.016 for the  $R$  band. We have checked the calibration using the surface brightness profiles of NGC 1199 shown in Mendes de Oliveira (1992) and no zero point differences were found. For NGC 6868 a similar procedure was applied using images from the Las Campanas Observatory 2.5–meter telescope and calibrated with Landolt (1992) standard stars. The RMS of these calibrations are 0.003 for the  $B$  band and 0.004 for the  $R$  band. In order to obtain the standard star photometry, we used the packages APPHOT and DAOPHOT.

### 2.2.2. Add-star experiments

We used each final image, with bright objects masked out, for an add-star experiment using the IRAF task ADDSTAR in the DAOPHOT package. Our goals were to evaluate the detection completeness, photometric errors and the limit of the Star–Galaxy (SG) separation method.

We added 600 artificial stellar-like objects to each 0.5 mag bin in the  $B$  image, covering the range  $18 < B < 28$ . In the  $R$  image we have added objects in the same position of the ones added to the  $B$  image, with  $(B - R)$  colors ranging randomly from 0 to 2.5. The objects were generated from the PSF for each field. The PSF was constructed using typically 40 to 80 point-sources found in the images. These artificial point sources were added in 30 runs of 20 objects each, to avoid artificial crowding of the field. Detection and photometry of the objects in the frames which contained the

artificial objects was then performed in the same manner done for the original images. The final simulated object list is composed by the simulated objects recovered in both bands. The number of objects which were recovered over the input number then gave us the completeness fraction. A comparison of the input and output magnitudes of the objects gave us estimates of the random and systematic uncertainties in the photometry.

We have determined the completeness fraction in radial rings centered on the galactic center, and this radial completeness fraction was the one applied in our analyses. This radial dependence is expected since the noise increases in the galaxy subtracted image as we get close to the center of the galaxy. The radial completeness fractions for both galaxies can be seen in figure 3. We have also studied the completeness as a function of color and found the variations being at most 5%.

As can be seen in figure 3, the SExtractor magnitudes are systematically too faint by  $\sim 0.05$  mag. This difference is expected and is due to the aperture correction applied by SExtractor being slightly underestimated for point sources (Bertin and Arnouts 1996). We applied a correction of this light loss to the photometry of detected objects in each of the frames. The completeness limit for our data given by the add-star experiment was considered to be the magnitude at which at least 50% of the objects were recovered and is shown in table 3.

### 3. Analysis and Results

#### 3.1. Globular Cluster Luminosity Function

In order to select the globular cluster candidates, we have restricted our samples to objects with  $22.0 < B < 25.5$  and  $20.0 < R < 24.0$  for NGC 1199 and  $22.0 < B < 24.5$  and  $20.0 < R < 23.0$  for NGC 6868, which represent the ranges of magnitudes where we expect to observe GCs (the faint limit is given by the completeness limit). We have also applied color limits  $0.7 < (B - R)_0 < 2.1$  which is the range where we expect to find the GCs (Thompson and Gregory 1993; Puzia *et al.* 1999; Woodworth and Harris 2000), eliminating very blue and red unresolved objects.

For our selected sample, we plot the number-density as a function of distance from the center of the galaxies (see figure 4). In those plots we can clearly see at which radius the background level for the objects was reached. Counting objects in rings of 0.2 arcmin, and correcting the counts by incompleteness, we can see that the radial profile reaches the background counts at distances larger than 2.4 arcmin from the center of NGC 1199. For NGC 6868 we have counted objects in rings of 0.5 arcmin. The counts in the background field (for radii greater than 10 arcmin in figure 4) are approximately constant and these are taken to represent the background counts for this group. The errorbars represent the poissonian error on the number counts.

We have used the flat region between  $2'.4$  (23 kpc) and  $4'.2$  (40 kpc) around NGC 1199 to estimate the background level. We do not have control fields taken away from the group center to make a background estimation in another way. From figure 4 we note that there is a central

concentration of objects within a radius of 2.4 arcmin from the center of NGC 1199. We identify this concentration with the GCS of this galaxy. A similar analysis was applied to NGC 1190 (HCG 22B) and NGC 1189 (HCG 22C) and no significant central concentration of point-like sources was found around them. From their morphological types (Sa and SBcd) and their luminosities ( $M_V = -18.7$  and  $M_V = -19.6$ , Hickson *et al.* 1989) they are not expected to have a large GC population (Harris 1991; Ashman and Zepf 1998).

We can also see a high concentration of objects around the center of NGC 6868, as is shown in figure 4. At galactocentric distances larger than 10 arcmin, 78 *kpc*, (objects located on the second field), we have a flat region which is used as the background control field. We regard as our sample of possible candidate globular clusters of NGC 6868 the objects within a distance of 3.8 arcmin (30 *kpc*) of the center of the galaxy (within the magnitudes and color limits previously defined). The objects within an annulus of inner radius of 10 arcmin and outer radius 17 arcmin were considered to belong to a sample of background galaxies and foreground stars (within the same limits).

We will, hereafter, refer to the area within 2.4 arcmin from the center of NGC 1199 and 3.8 arcmin from the center of NGC 6868 as the “on-galaxy region” or “studied area” and to the region within 2.4 and 4.2 arcmin from the center of NGC 1199 and the field taken 10 arcmin from the center of NGC 6868 as the “background area”.

Since we do not have an independent background field for NGC 1199, we have estimated the number of foreground stars in the direction of the galaxy using the galactic model by Santiago, Gilmore and Elson (1996). We found that in the magnitude range of the globulars, the possible contamination of our sample by foreground stars is 0.4 objects/arcmin<sup>2</sup>, which gives us only 5.5 objects in the studied area. This foreground stars estimate is negligible and the number of GCs found around NGC 1199 could not be much affected by a wrong stellar contamination estimate in our small area background field. However, by far the largest source of contamination is by background galaxies. The background field used for NGC 1199 (the outskirts of the field) gives a statistically more uncertain background subtraction and can still contain bona-fide GCs that will be counted as background objects (although figure 4 shows a very flat profile beyond a distance of 2.4 arcmin from the center of the galaxy). In the case of NGC 6868, since the estimate of the number of foreground/background objects was done using an independent frame of same size as the on-galaxy frame, obtained at a distance of 10 arcmin to the center of the galaxy, the background subtraction is more reliable.

The globular cluster luminosity function (GCLF) was built binning the GC candidates to 0.5 magnitude. The number counts were corrected for incompleteness dividing the number counts of each bin by the completeness fraction. The photometric errors were neglected and the errors for the corrected number counts were given by

$$\sigma^2 \approx \left[ \frac{N_{obs}}{f^2} + \frac{(1-f)N_{obs}^2}{N_{add}f^3} \right] \quad (1)$$

(Bolte 1994), where  $N_{obs}$  is the number of objects detected in the image,  $N_{add}$  is the number of objects added to the image in the addstar-experiment and  $f$  is the completeness fraction to this magnitude bin.

The corrected number counts for the on-galaxy region were subtracted by the corrected background number counts normalized to the sampled area. For NGC 1199, we have selected  $128 \pm 11$  objects, which corrected for incompleteness gives  $158 \pm 14$  objects, in an area of  $13.7 \text{ arcmin}^2$ . In the background, for the same area, we have a corrected number count of  $61 \pm 10$  objects, leaving a net number count of  $97 \pm 18$  objects. For NGC 6868, there are  $111 \pm 10$  selected objects, which corresponds to  $124 \pm 12$  objects when corrected for incompleteness, in an area of  $27.2 \text{ arcmin}^2$ . In the background we have a corrected number count of  $74 \pm 8$  objects in the same area resulting in a net number count of  $50 \pm 14$  objects.

The luminosity function of globular clusters around giant elliptical galaxies has been well studied in the literature. It is generally accepted that it can be well approximated by a Gaussian distribution function. For the peak (turnover magnitude  $-m_0$ ) and the dispersion we have used the typical values for elliptical galaxies  $M_V = -7.33 \pm 0.04$  and  $\sigma = 1.40 \pm 0.05$  (Harris 2001).

The galactic extinction is the same for both galaxies,  $E(B - V) = 0.056$  (Schlegel, Finkbeiner and Davis 1998). With the reddening laws found in Rieke and Lebofsky (1985) we have  $A_B = 0.23$ ,  $A_R = 0.13$  and  $E(B - R) = 0.10$ .

Using the distance moduli for our galaxies and the reddening corrections above, we expect to start seeing the brightest GCs for NGC 1199 at  $B = 22.5$  and  $R = 20.9$  and the turnover at  $B = 26.2 \pm 0.3$  and  $R = 24.6 \pm 0.3$ . For NGC 6868,  $B = 22.1$  and  $R = 20.5$  for the brightest GCs and  $B = 25.7 \pm 0.2$  and  $R = 24.1 \pm 0.2$  for the turnover magnitude. As we do not reach the turnover point of the GCLF with our data, we did not attempt to fit the peak and the dispersion values, leaving only the normalization of the Gaussian as a free parameter. The  $\chi^2$  of the fits and the area of the Gaussians covered by our data for both galaxies are seen in table 4 and figure 5.

### 3.2. Specific Frequency and Radial Profile Modeling

The specific frequency ( $S_N$ ), as defined by Harris and van den Bergh (1981), is the number of objects normalized by the galaxy luminosity.

$$S_N \equiv N_{GC} 10^{0.4(M_V + 15)} \quad (2)$$

Using a Gaussian fit for the GCLF we can determine the part of the GC population that we are measuring and extrapolate the number of GCs over all magnitudes in our image. With the number of GCs found in the on-galaxy areas (local number) and the light in the same area where the GCs were counted, we can calculate the “local specific frequency” ( $S_{N_l}$ ), *i.e.*, the specific frequency of



the GCs that are detected in our images.

Correcting the number counts of NGC 1199 for the unobserved part of the GCLF we have a total number of  $314 \pm 105$  GCs over all magnitudes. The galaxy light, estimated using the ELLIPSE model in the same area, is  $V = 12.9 \pm 0.2$  or  $M_V = -19.9 \pm 0.3$ . Using those values to calculate the local specific frequency ( $S_{N_l}$ ) for NGC 1199 we have  $3.4 \pm 1.5$ . Applying the same procedure for NGC 6868 the local number of GCs over all magnitudes is  $266 \pm 106$  and the light in this area is  $V = 11.0 \pm 0.2$  or  $M_V = -21.3 \pm 0.3$ , which gives a  $S_{N_l} = 0.8 \pm 0.4$ . The errors on  $S_N$  include the error on the number counts, background subtraction, GCLF extrapolation and its parameters uncertainties, the photometric error on the galaxy magnitude and the error in the distance of the galaxy.

We now determine the global specific frequency ( $S_{N_g}$ ) for the system.  $S_{N_g}$  is calculated using the extrapolation of the radial profile to estimate a total number of GCs for each galaxy and the total light of the galaxy.

To estimate the total number of objects in the GCS, the sample was divided in radial rings of 0.2 arcmin for NGC 1199 and 0.5 arcmin for NGC 6868. The number of GC candidates in each radial ring was corrected by the lost area due to the masks and unobserved regions. We then calculated the total number of GCs over all magnitudes in the complete ring from the central mask and the limiting galactocentric distance. We use two different radial profiles. The first one is a variation of the “core model” profile proposed by Forbes *et al.* (1996) ( $\rho = \rho_0(r_c^\alpha + r^\alpha)^{-1}$ ) with the core radius estimated for the GCSs of elliptical galaxies by the relation shown in the same work ( $r_c(kpc) = -(0.62 \pm 0.1) \cdot M_V - 11.0$ ). This “core model” profile is a simplified analytic form for the King profile (King 1962). The other profile is a power-law profile ( $\rho \propto r^{-\alpha}$ ).

For either profile the best-fitting model was determined and the total number of GC estimated by integrating the profiles. For NGC 1199 the profile was constrained by the corrected number counts between 0.45 and 2.4 arcminutes. For NGC 6868 the fitted range was 0.35 to 3.8 arcminutes. Table 5 and figure 6 summarize the fits.

For NGC 1199 the slope of the power-law profile is  $2.5 \pm 0.3$ , which is very steep and therefore the total number of GCs is dominated by the central region. To be able to integrate this profile, we have set a minimum inner radius of 0.1 arcmin ( $\sim 1 kpc$ ). We assume that there is no contribution inside this radius since the GCs in this region were probably destroyed by erosion processes. This mathematical artifact gives an upper limit of the total population of GCs. For NGC 6868 the slope of the best-fit power-law profile is  $1.4 \pm 0.3$  and it can be integrated analytically (see results below). The slopes used in the “core model” profile are the same used in the power-law profile.

The total number of GCs for each galaxy estimated by the two kinds of profiles can be seen in table 5, and the radial profiles of GC candidates with the power-law and “core model” profiles used and the galaxy light overplotted are shown in figure 6. The assumption on the profile shape is very important because we have to extrapolate the number counts in the outer and inner parts of the galaxy.

The profiles were extrapolated to 100 *kpc*, which is the maximum radius we expect the GCS to extend. Rhode and Zepf (2001) do not detect GCs farther than 100 *kpc* in NGC 4472, which is at least twice as luminous as the galaxies in our sample. Three sources of error were considered on the radial profile extrapolation using the “core model”: the errors on the slope, on the core radius and on the outer radius cut-off. To estimate the error we make by cutting the profiles at the outer radius (100 *kpc*) we have calculated the variation of the results by varying the outer radius cut-off by 20%. For NGC 1199, where the numbers are dominated by the inner region, the error on the  $S_N$  is 0.06 and for NGC 6868 is of 0.2. The error introduced in the  $S_N$  by a 30% variation of the core radius is of 0.6 for NGC 1199 and only 0.04 for NGC 6868, where the numbers are dominated by the outer region.

For the extrapolation using the power-law profile three sources of error were also considered: the error on the slope and on the outer radius cut-off, in the same manner as for the “core radius” extrapolation, and the error on the inner radius cut-off, for the case of NGC 1199. We have varied the inner radius cut-off (1 *kpc*) by 50% to estimate the error we make on the cut, which translated into an error for the  $S_N$  of 1.8. The errors caused by all the sources, for both models, were added in quadrature and are shown in table 5.

To calculate the  $S_{N_g}$  we have used the total magnitude of the galaxies and the total number of GCs obtained through the integration of the two kinds of profiles. The results are shown in table 5 and are discussed in section 4.

### 3.3. GC Color Distribution

Bimodal color distributions of GCs are found in at least 50% of elliptical galaxies (Gebhardt and Kissler-Patig 1999; Kundu and Whitmore 2001) and even in some spiral galaxies like our own and M31 (Ashman and Zepf 1998; Harris 2001, and references there in). They are thought to be due to multiple events of star formation in the galaxies’ histories. This effect was predicted in elliptical galaxies by Ashman and Zepf (1992) merger model, first detected in NGC 4472 and NGC 5128 (Zepf and Ashman 1993) and since then other models appeared to explain it, like the multiple collapse model (Forbes, Brodie and Grillmair 1997) and the accretion model (Côté, Marzke and West 1998; Hilker, Infante and Richtler 1999). Since we are searching for modifications on the GCS properties caused by the small group environment, multimodal color distributions of GCs may give some useful information about the GCS history.

The color distribution of all the objects detected in the on-galaxy areas is analyzed here, with no attempt to perform a background subtraction. The color distributions of the background objects, which can be seen in figure 7, are very broad with one dominant peak. The peak positions are not located at the same place as the GCs candidates peaks (see figure 8). Therefore, we do not expect the shape of the background color distribution to affect our analysis.

We have applied a KMM test (Ashman, Bird and Zepf 1994) to detect and estimate the param-

eters of possible bimodalities in the color distributions. The KMM code uses maximum likelihood to estimate the parameters that best describe the sample distributions for a single Gaussian and for multiple Gaussian fits and calculates the probability of the single Gaussian being the best fit for the sample distribution. This code can be run in two modes, homoscedastic, which finds groups with the same covariance values, and heteroscedastic, which finds groups with dissimilar covariance values. The last mode has reliability problems with the analytic approximation to the significance level and for this reason it is not commonly used for this kind of analysis.

Running KMM on our color distributions, with the homoscedastic case, yields the two-Gaussian option as the result with 99.9% confidence level for both galaxies. For NGC 1199 the peaks are located at  $(B - R)_0 = 1.13 \pm 0.04$  and  $(B - R)_0 = 1.42 \pm 0.04$  with 62% of the GCs on the blue peak and 38% on the red one and a covariance of 0.01. For NGC 6868 the values found are  $(B - R)_0 = 1.12 \pm 0.07$  and  $(B - R)_0 = 1.42 \pm 0.07$  with 51% of the GCs on the blue peak and 49% on the red peak and a covariance of 0.009. The errors represent the mean error on the peak position given by the KMM added in quadrature with the mean photometric errors of the colors.

A visual inspection of the color histograms and the estimates using the Epanechnikov kernel density estimator (see Silverman 1986, for detailed discussion on the kernel density estimator) shows that there might be a bimodality for NGC 1199 and that there are, at least, two major peaks for NGC 6868. The KMM results, bimodality significance and the peak positions, are in good agreement with the visual inspections and the kernel density estimates, as can be seen in the distributions in figure 8.

Splitting the GC candidates into blue and red sub-samples, we have analyzed the radial distribution of each sub-population and found that the red clusters are more centrally concentrated than the blue ones, as found in the literature (Geisler, Lee and Kim 1996; Kissler-Patig *et al.* 1997; Lee, Kim and Geisler 1998; Kundu and Whitmore 1998). The slopes found fitting a power-law to the radial profiles are  $2.2 \pm 0.4$  and  $2.9 \pm 0.6$  to the blue and red sub-populations of NGC 1199, respectively, and  $0.8 \pm 0.4$  and  $1.7 \pm 0.2$  to the blue and red sub-populations of NGC 6868, respectively.

#### 4. Discussion and Conclusions

We present a short summary of the results we have found so far before we proceed with the discussion:

(1) We detect a significant population of centrally concentrated GCs around the galaxies NGC 1199 and NGC 6868, as shown in figure 4.

(2) The two first-ranked group galaxies studied here show different  $S_N$  values. For NGC 1199, the  $S_N$  appears to be “normal” for an elliptical galaxy, while for the suspected merger NGC 6868, the specific frequency is somewhat low compared to other galaxies of similar luminosities.

(3) We find a good case for bimodal color distributions in the populations of GCs and in both cases the radial distributions for the red objects have steeper slopes than those for the blue objects.

In the following we will further discuss these main results and will attempt to fit our observations into what is known about GC systems around other elliptical galaxies.

#### 4.1. Radial profiles and population sizes

The radial profiles shown in figure 4 show a central concentration of objects within 2.4 arcmin (23 *kpc*) of the center of NGC 1199 and 3.8 arcmin (30 *kpc*) of the center of NGC 6868, indicating the existence of a significant population of globular clusters around these galaxies.

NGC 1199 has a very steep radial profile that follows the galaxy light and can be fitted by a power-law with  $\alpha = 2.5 \pm 0.3$  and by a “core model” profile with the same slope and a core radius of  $r_c = 2.19$  *kpc*. The light profile of NGC 1199 is as steep as the radial distribution of GCs out to a radius of 1.5 arcmin and then it becomes steeper. Using our determination of the global specific frequency for this galaxy done with the “core model” profile, our value of  $S_N$  can only be taken as an upper limit, if the real profile of the GCSs follows the light of the galaxy exactly. The steep profile can be caused by the destruction of the outer part of the system by tidal effects, since we have two giant galaxies closer than 35 *kpc* and with small relative velocities, or by some inefficiency of the erosion processes in the inner part of the galaxy. The global specific frequency estimated ( $3.6 \pm 1.8$  using the “core model” and  $5.2 \pm 3.2$  using the power-law model) is similar to the “normal” value for elliptical galaxies, where the “normal” value is defined as a typical value for elliptical galaxies as given by Harris (2001). There is no optical sign of star formation regions in the galaxy that could artificially change the  $S_N$  value.

The GCS of NGC 6868 has a regular radial profile, the slope of the power-law fitted to the distribution is  $\alpha = 1.4 \pm 0.3$ . The slope value for a power-law radial profile of GCs for a normal elliptical galaxy ranges from 1 to 2 (Ashman and Zepf 1998). The GCS profile is more extended than the galaxy light, which has a slope of 1.72, as can be seen in figure 6. Our final result for the global specific frequency for this galaxy is  $S_N = 1.8 \pm 1.1$ , assuming a “core model” profile, and  $1.9 \pm 1.0$ , assuming the power-law profile. This value is lower, by almost a factor of two, than the “normal” value of Harris (2001) for an elliptical galaxy ( $S_N \sim 3.5$ ) and indicates a poor GCS (although it’s well known that the scatter on the values of  $S_N$  for elliptical galaxies is large). This might be due to a high efficiency of forming stars in the past as opposed to the formation of globular clusters or to very efficient destruction mechanisms that could perhaps be related to the recent merger that may have occurred in the central part of the galaxy (Hansen *et al.* 1991). As for NGC 1199, there are no obvious signs of wide-spread star formation throughout the galaxy that could affect the  $S_N$  value of NGC 6868.

## 4.2. Colors of the GC population

According to stellar population evolutionary synthesis models (Worthey 1994; Bruzual and Charlot 1993) metallicity effects are supposed to dominate color differences in globular clusters if the populations are older than 1 Gyr. We expect the bulk of the populations of GCs to be older than 1 Gyr, since we could not find evidences of recent star formation. A linear relation between the color and the metallicity is predicted by the population synthesis models as the relation proposed by Reed, Harris and Harris (1994) ( $[Fe/H] = 3.112(B - R)_0 - 4.967$   $\sigma[Fe/H] = 0.21$ ).

Some studies have found doubly-peaked color distributions of GCSs around elliptical galaxies. Gebhardt and Kissler-Patig (1999) and Kundu and Whitmore (2001) found for samples of respectively 43 and 29 early-type galaxies observed with HST, that at least 50% of the elliptical galaxies have GCSs with bimodal color distributions. Studies of the GCS of NGC 4472 (M49) (Geiser *et al.* 1996; Lee *et al.* 1998; Puzia *et al.* 1999) have found color distributions with peak metallicities corresponding to  $[Fe/H] = -1.5 \pm 0.05$  dex and  $[Fe/H] = -0.32 \pm 0.05$  dex, using the color-metallicity relation given by Kundu and Whitmore (1998) ( $[Fe/H] = -(4.50 \pm 0.30) + (3.27 \pm 0.32) \cdot (V - I)$ ). Neilsen and Tsvetanov (1999), in a study of 12 Virgo elliptical galaxies found a bimodal color distribution for the GCSs around 8 of them.

The recent work of Larsen *et al.* (2001), presents an analysis of 17 nearby early-type galaxies, homogeneously observed with HST. In this work they have found a correlation between the GCS mean color and the luminosity and the mean color and the velocity dispersion of the host galaxy. Strong correlations were found for the red peaks, which were also found by Forbes *et al.* (1997) and by Forbes and Forte (2001). The latter study suggested the following color-velocity dispersion relation  $(V - I) = 0.23 \cdot \log\sigma + 0.61$ . Weak correlations were found for the blue peaks and were discarded by the previously cited works. Burgarella, Kissler-Patig and Buat (2001) have found an average metallicity of  $[Fe/H] = -1.4$  dex for the blue peak, which agrees with the average value found previously by other authors. Kundu and Whitmore (2001) found that the correlations for both peaks are, at best, weak. In general, the average metallicity of the globular clusters on a bimodal-distribution, when considered as a single population, is in agreement with the value of a unimodal distribution ( $[Fe/H] = -1.0 \pm 0.05$  dex, Kundu and Whitmore 2001).

The GCSs around the two galaxies studied here were analyzed with the the KMM code (Ashman *et al.* 1994) which has detected bimodal populations for the GCSs around NGC 1199 and NGC 6868.

For NGC 1199, KMM has located peaks at  $(B - R)_0 = 1.13 \pm 0.04$  and  $(B - R)_0 = 1.42 \pm 0.04$ , which corresponds to  $[Fe/H] = -1.45 \pm 0.21$  dex and  $[Fe/H] = -0.55 \pm 0.21$  dex, respectively (Reed *et al.* 1994), similar to the values were found for many published galaxies in the last years, as seen in the following. Transforming our  $(B - R)$  values to  $(V - I)$ , using the relation given by Forbes and Forte (2001) ( $(V - I) = 0.68(B - R) + 0.15$ ), and overplotting them (large filled symbols) on the Forbes and Forte (2001) color-velocity dispersion plot (figure 9), we can see that our results are consistent with theirs and those of other studies.

For NGC 6868, peaks found by KMM are located at  $(B - R)_0 = 1.12 \pm 0.07$  and  $(B - R)_0 = 1.42 \pm 0.07$ , corresponding to  $[Fe/H] = -1.48 \pm 0.22 \text{ dex}$  and  $[Fe/H] = -0.55 \pm 0.22 \text{ dex}$ , respectively (Reed *et al.* 1994). Those values are also in agreement with the ones found for many galaxies in the literature. In figure 9 we can see our measured values overplotted onto the diagram of Forbes and Forte (2001) (large open symbols).

The results reported in this work show that there is a need of more work on globular cluster systems around small-group elliptical galaxies in order to understand the effects to which the GCSs are exposed in such environment.

CDR is supported by FAPESP (Fundação de Amparo a Pesquisa do Estado de São Paulo) PhD. grant No. 96/08986–5. CMO acknowledges support from FAPESP (Fundação de Amparo a Pesquisa do Estado de São Paulo). MB is happy to acknowledge support from National Science Foundation grant AST 99-01256. BLZ acknowledges support from the Deutsche Forschungsgemeinschaft (DFG) and the VW foundation. THP gratefully acknowledges the financial support during his visit at Universidade de São Paulo. We are grateful to Mike West, Basílio Santiago, Arunav Kundu and Keith Ashman, the paper referee, for the careful reading of this manuscript and useful comments to improve its content and to Héctor Cuevas and Leopoldo Infante for observing the standard stars for calibration of the NGC 6868 field.

## REFERENCES

- Ashman, K. M., Bird, C. M. and Zepf, S. E. 1994, *AJ*, 108, 2348
- Ashman, K. M. and Zepf, S. E. 1992, *ApJ*, 384, 50
- Ashman, K. M. and Zepf, S. E. 1998, *Globular Cluster Systems*, Cambridge University Press
- Bertin, E. and Arnouts, S. 1996, *A&A*, 117, 393
- Beuing, J., Döbereiner, S., Böhringer, H. and Bender, R. 1999, *MNRAS*, 302, 209
- Bolte, M. 1994, *ApJ*, 431, 223
- Bridges, T. J., Carter, D., Harris, W. E. and Pritchett, C. J. 1996, *MNRAS*, 281, 1290
- Bruzual, G. A. and Charlot, S. 1993, *ApJ*, 405, 538
- Burgarella, D., Kissler-Patig, M. and Buat, V. 2001, *AJ*, 121, 2647
- Côté, P., Marzke, R. O. and West, M. J. 1998, *ApJ*, 501, 544
- de Vaucouleurs, G., de Vaucouleurs, A., Corwin, H. G., Buta, R. J., Paturel, G. and Fouqué, P. 1991, *Third Reference Catalogue of Bright Galaxies*, Springer Verlag, New York (RC3)

- Djorgovski, S. and Santiago, B. X. 1992, *ApJ*, 391, 85
- Elmegreen, B. 2000, “Toward a New Millennium in Galaxy Morphology”, eds. D. L. Block, I. Puerari, A. Stockton and D. Ferreira, 1999, (Kluwer, Dordrecht) *ApSpSc*, 269/270, 469
- Faber, S., Wegner, G., Burnstein, D. Davies, R. L., Dressler, A., Lynden-Bell, D. and Terlevich, R. J. 1989, *ApJS*, 69, 763
- Forbes, D. A., Brodie, J. P. and Grillmair, C. J. 1997, *AJ*, 113, 1652
- Forbes, D. A. and Forte, J. C. 2001, *MNRAS*, 322, 257
- Forbes, D. A., Franx, M., Illingworth, G. D. and Carollo, C. M. 1996, *ApJ*, 467, 126
- Gebhardt, K. and Kissler-Patig, M. 1999, *AJ*, 118, 1526
- Geisler, D., Lee, M. G. and Kim, E. 1996, *AJ*, 111, 1529
- Hansen, L., Jørgensen, H. E. and Nørgaard-Nielsen, H. U. 1991, *A&A*, 243, 49
- Harris, W. E. 1991, *ARA&A*, 29, 543
- Harris, W. E. 2001, “Globular Cluster Systems”, Lectures for the 1998 Saas-Fee Advanced School on Star Clusters (Course 28), eds. L. Labhardt and B. Binggeli, Springer (Berlin), 223
- Harris, W. E. and van den Bergh, S. 1981, *AJ*, 86, 1627
- Hickson, P. 1982, *ApJ*, 255, 382
- Hickson, P., Kindl, E. and Auman, J. R. 1989, *ApJS*, 70, 687
- Hickson, P., Mendes de Oliveira, C., Huchra, J. P. and Palumbo, G. G. 1992, *ApJ*, 399, 353
- Hilker, M., Infante, L. and Richtler, T. 1999, *A&AS*, 138, 55
- King, I. R. 1962, *AJ*, 67, 471
- Kissler-Patig, M., Richtler, T., Storm, J. and Della Valle, M. 1997, *A&AS*, 327, 503
- Kobayashi, C. and Arimoto, N. 2000, *ApJ*, 527, 573
- Kron, R. G. 1980, *ApJS*, 59, 115
- Kundu, A. and Whitmore, B. C. 1998, *AJ*, 116, 2841
- Kundu, A. and Whitmore, B. C. 2001, *AJ*, 121, 2950
- Landolt, A. U. 1992, *AJ*, 104, 340
- Larsen, S. S., Brodie, J. P., Huchra, J. P., Forbes, D. A. and Grillmair, C. 2001, *AJ*, 121, 2974

- Lee, M. G., Kim, E. and Geisler, D. 1998, *AJ*, 115, 947
- Mendes de Oliveira, C. L. 1992, PhD. Thesis, Univ. of British Columbia
- Neilsen, E. H. and Tsvetanov, Z. I. 1999, *ApJ*, 515L, 13
- Oke, J. B., Cohen, J. G., Carr, M., Cromer, J., Dingizian, A., Harris, F. H., Labrecque, S., Lucinio, R., Schaal, W., Epps, H. and Miller, J. 1995, *PASP*, 107, 375
- Plana, H., Boulesteix, J., Amram, Ph., Carignan, C. and Mendes de Oliveira, C. 1998, *ApJS*, 128, 75
- Prugniel, P. and Simien, F. 1996, *A&A*, 309, 749
- Puzia, T. H., Kissler-Patig, M., Brodie, J. P. and Huchra, J. P. 1999, *AJ*, 118, 2734
- Reed, L. G., Harris, G. L. H. and Harris, W. E. 1994, *AJ*, 107, 555
- Rhode, K. L. and Zepf, S. E. 2001, *AJ*, 121, 210
- Rieke, G. H. and Lebofsky, M. J. 1985, *ApJ*, 288, 618
- Santiago, B. X., Gilmore, G. and Elson, R. A. W. 1996, *MNRAS*, 281, 871
- Schlegel, D. J., Finkbeiner, D. P. and Davis, M. 1998, *ApJ*, 500, 525
- Silverman, B. W. 1986, *Density Estimation for Statistics and Data Analysis* (New York:Springer), 18
- Tonry, J. L., Dressler, A., Blakeslee, J. P., Ajhar, E. A., Fletcher, A. B., Luppino, G. A., Metzger, M. R. and Moore, C. B. 2001, *ApJ*, 546, 681
- Thompson, L. A. and Gregory, S. A. 1993, *AJ*, 106, 2197
- Woodworth, S. C. and Harris, W. E. 2000, *ApJ*, 533, 137
- Worthey, G. 1994, *ApJS*, 95, 107
- Zepf, S. E. and Ashman, K. M. 1993, *MNRAS*, 264, 611
- Zepf, S. E. and Whitmore, B. C. 1993, *ApJ*, 418, 72
- Zepf, S. E., Geisler, D. and Ashman, K. M. 1994, *ApJ*, 435, 117



Fig. 1.— The left panels show the combined images for HCG 22 (upper panel) and NGC 6868 (lower panel) in the  $R$  band. The right panels show the final background subtracted masked images for HCG 22 (upper panel) and NGC 6868 (lower panel) where the detection and photometry were performed. The field sizes for the upper panels are  $5.7 \times 7.3$  arcmin and  $6.4 \times 6.4$  arcmin for the lower panels.

Fig. 2.— Magnitude–FWHM plane used to select point–like sources. The filled circles are the objects classified as point–like sources and the open circles are the objects classified as extended objects. Panel (a) shows the objects detected in the NGC 1199 images. Panel (b) shows the objects detected in the NGC 6868 images.

Fig. 3.— The left panels show the detection completeness fractions estimated with the add–star experiment performed in the six images of our study. Panels (a) and (b) give the total and radial completeness fractions for the HCG 22 images in the  $B$  and  $R$  bands, respectively. Panels (c) and (d) give the fractions for the NGC 6868 images in the  $B$  and  $R$  bands and panels (e) and (f) give the total completeness fraction for the NGC 6868 background fields in the  $B$  and  $R$  bands, respectively. The right panels show the photometric errors estimated with the add–star experiment. Panels (g) and (h) give the errors for the HCG 22 images in the  $B$  and  $R$  bands, respectively. Panels (i) and (j) for the NGC 6868 images and (k) and (l) for the NGC 6868 background fields in the  $B$  and  $R$  bands, respectively. The vertical dashed lines in the left panels mark the faint magnitude limit considered in each sample.

Fig. 4.— Radial profile of objects classified as point–like sources within the magnitudes and color limits ( $0.7 \leq (B - R)_0 \leq 2.1$ ). Panel (a) shows the distribution of objects around NGC 1199, from 0 to 6 arcmin in rings of 0.2 arcmin. The magnitude ranges are  $B = 22.0$  to  $25.5$  and  $R = 20.0$  to  $24.0$ . Panel (b) shows the distribution of objects around NGC 6868, from 0 to 17 arcmin in rings of 0.5 arcmin. The magnitude ranges are  $B = 22.0$  to  $24.5$  and  $R = 20.0$  to  $23.0$ . The solid lines represent the estimated background level: 4.2 objects/arcmin<sup>2</sup> for NGC 1199 and 2.4 objects/arcmin<sup>2</sup> for NGC 6868. Note the different scales for the upper and lower panel.

Fig. 5.— Globular cluster luminosity functions. Panel (a) shows the luminosity function of the globular cluster system around NGC 1199 in the  $B$  band and panel (b) in the  $R$  band. Panels (c) and (d) show the luminosity function of the globular cluster system around NGC 6868 in the  $B$  and  $R$  band respectively. The solid line represents de Gaussian fit and the dashed lines are the expected turnover magnitudes.

Fig. 6.— Radial profiles of globular cluster candidates. Panel (a) shows the radial profile of the candidates around NGC 1199 with the fitted “core model” profile with the best–suited core radius (Forbes *et al.* 1996) (dashed line) and the galaxy light in the  $B$  band arbitrarily vertically shifted (continuous line) overplotted. Panel (b) shows the radial profile of the GCS around NGC 1199 and the galaxy light (continuous line) with the power–law profile (dashed line) overplotted. Panels (c) and (d) show the same information of panels (a) and (b), respectively, for the candidates around

NGC 6868.

Fig. 7.— Color distribution of background objects. Panel (a) shows the color distribution of objects in the background area of NGC 1199 and panel (b) of those in the background area of NGC 6868. The solid line represents the distribution function derived by the Epanechnikov kernel density estimator and the dotted lines are its upper and lower limits.

Fig. 8.— Color distribution of globular cluster candidates (no background subtraction is done). Panel (a) shows the color distribution of objects around NGC 1199 and panel (b) of those around NGC 6868. The solid line represents the distribution function derived by the Epanechnikov kernel density estimator and the dotted lines are its upper and lower limits. The vertical dashed lines represent the peak values found by KMM.

Fig. 9.— Color–velocity dispersion relation for the early–type galaxies of Forbes and Forte (2001). Panel (a) shows the values for the red peaks and panel (b) for the blue peaks. The solid line represents the color–velocity dispersion relation proposed by Forbes and Forte (2001). The filled pentagons are the values for NGC 1199 and the open ones are the values for NGC 6868.

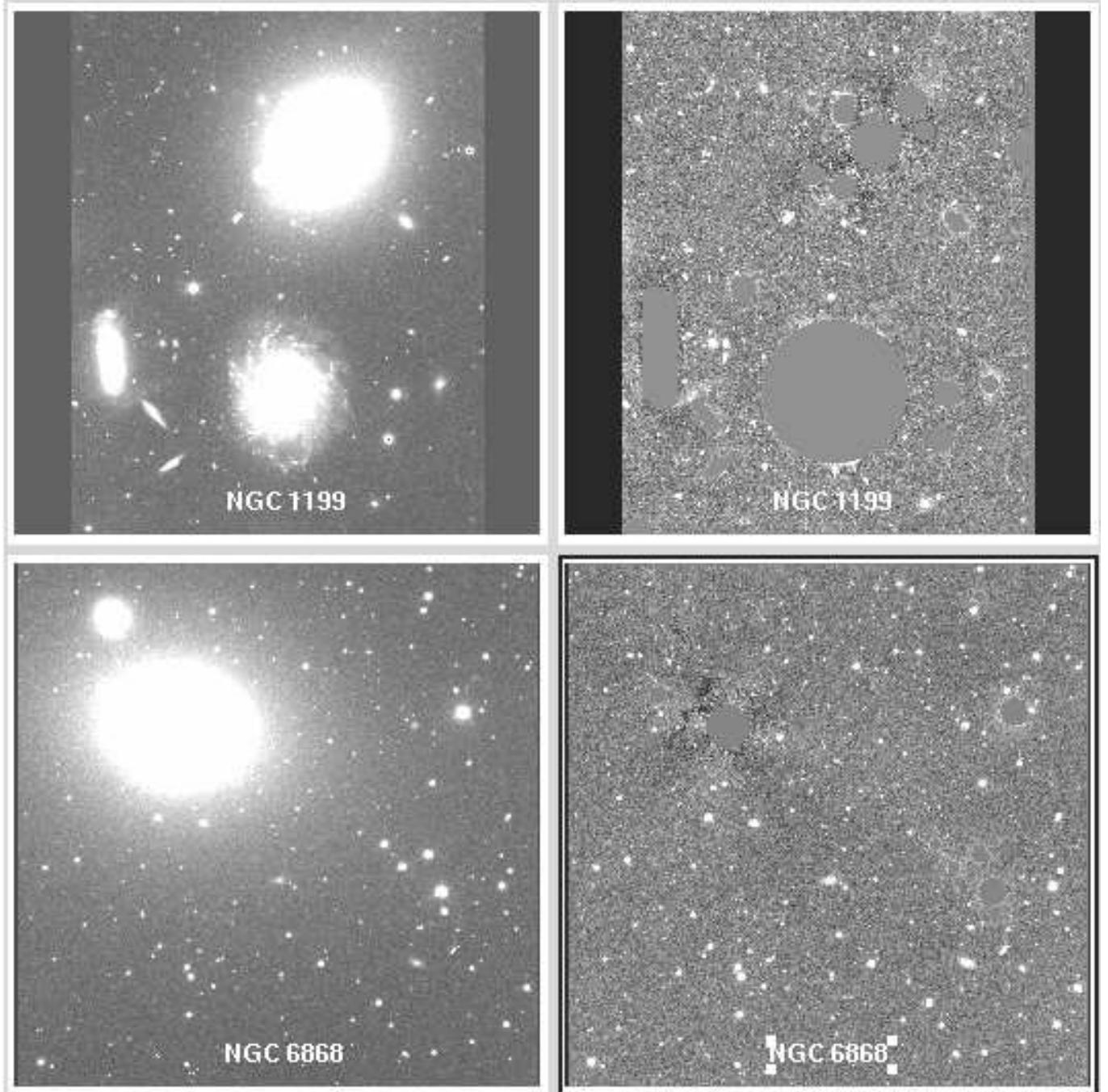


Figure 1.

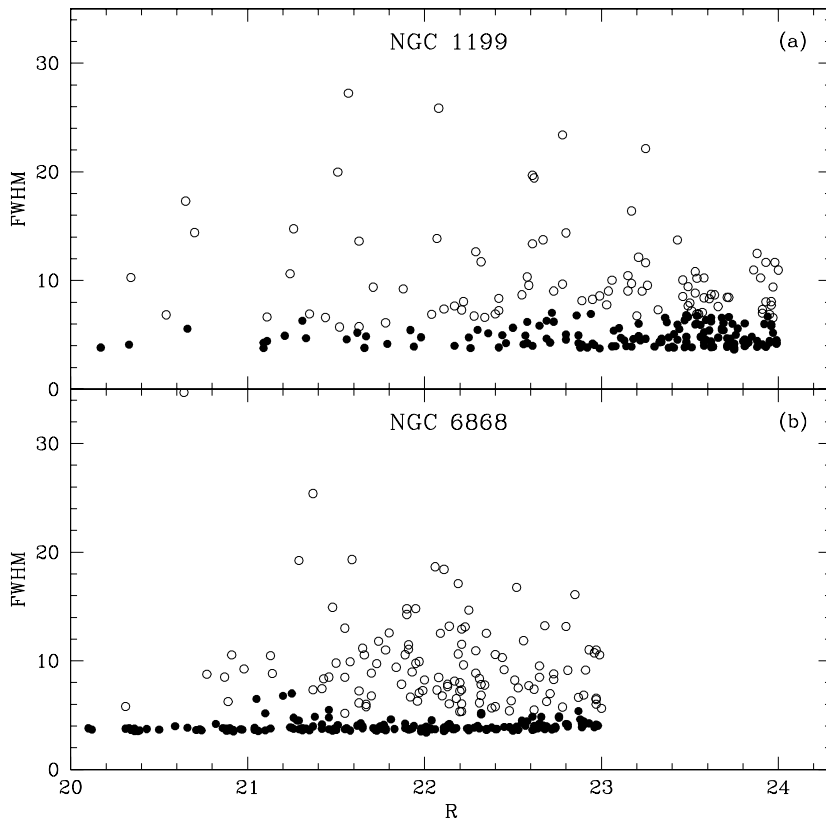


Figure 2.

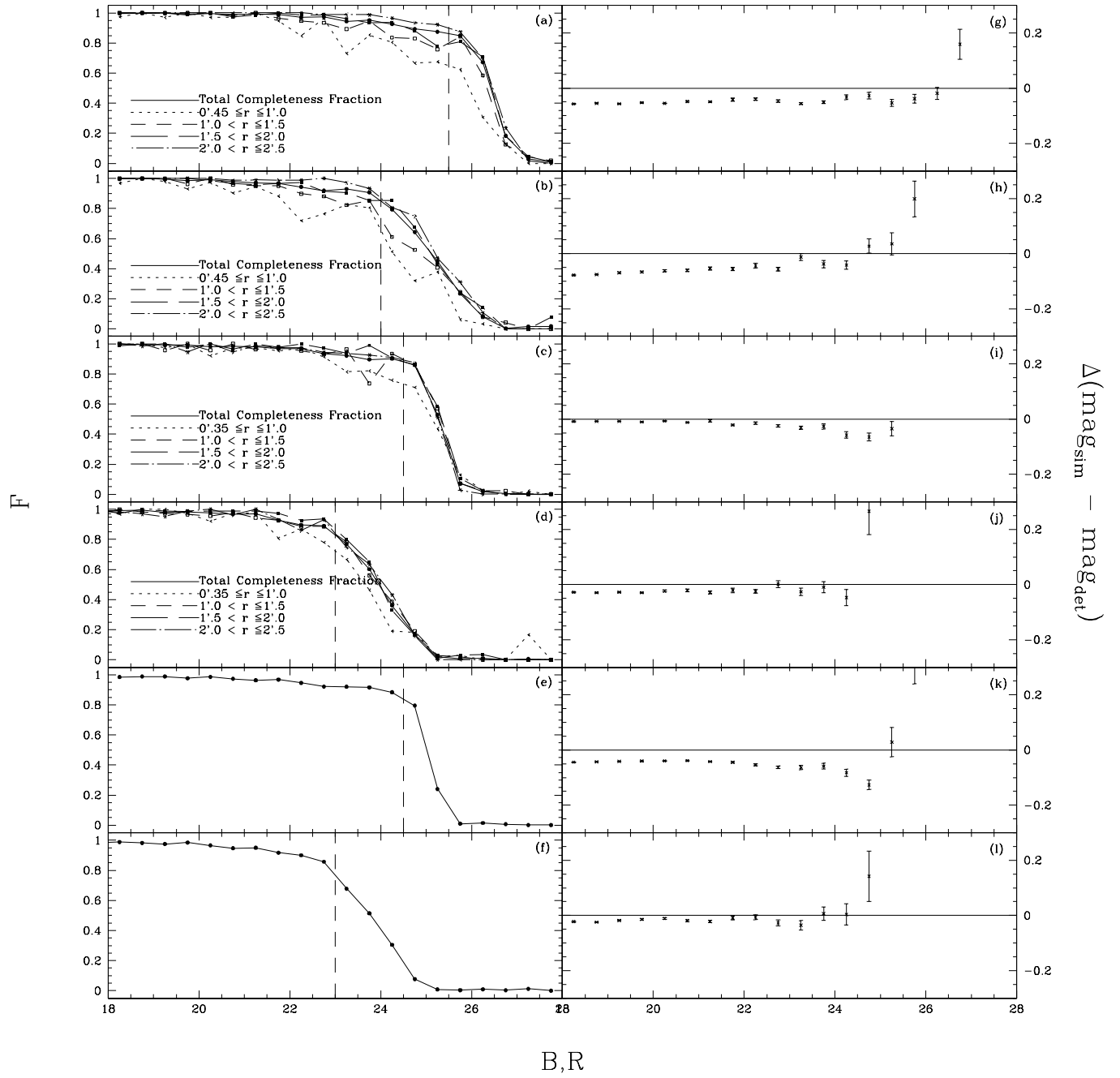


Figure 3.

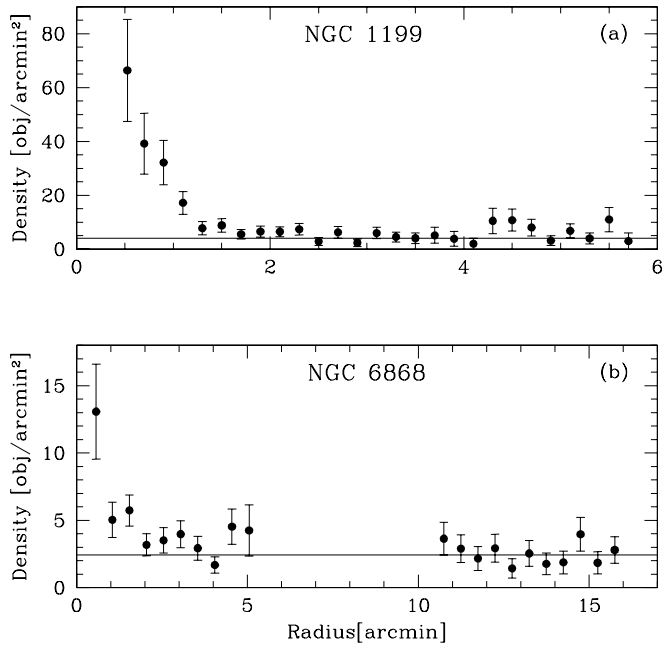


Figure 4.

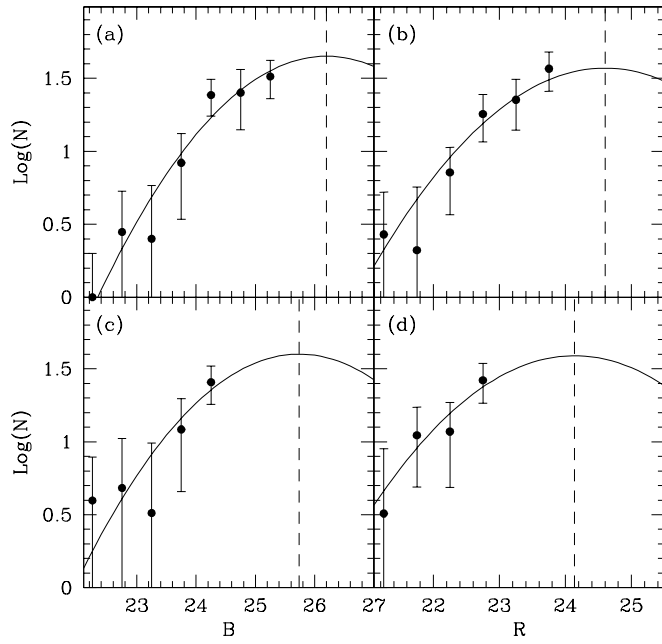


Figure 5.

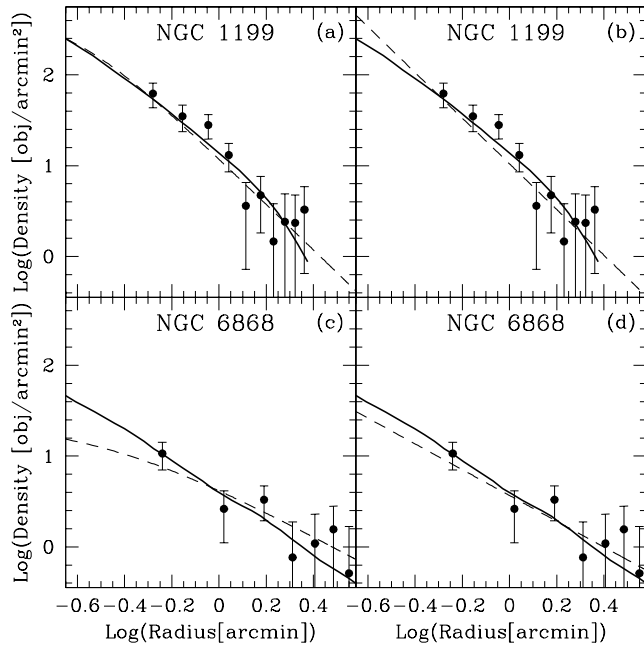


Figure 6.



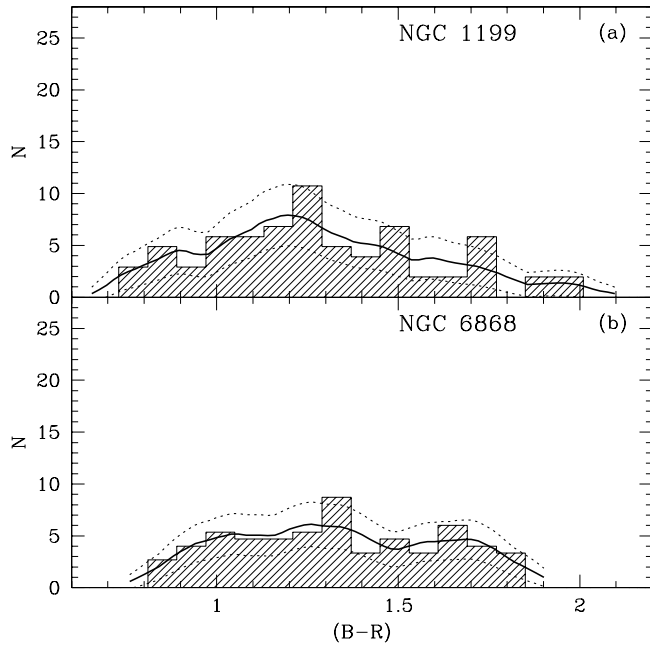


Figure 7.

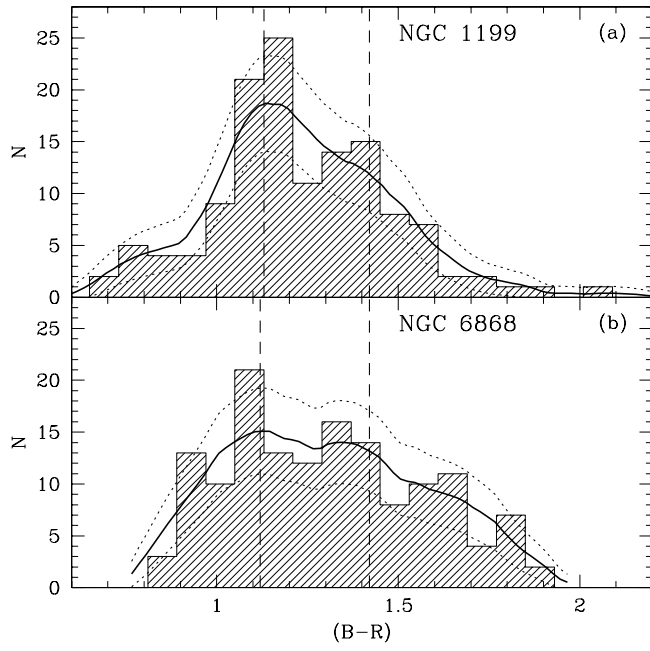


Figure 8.

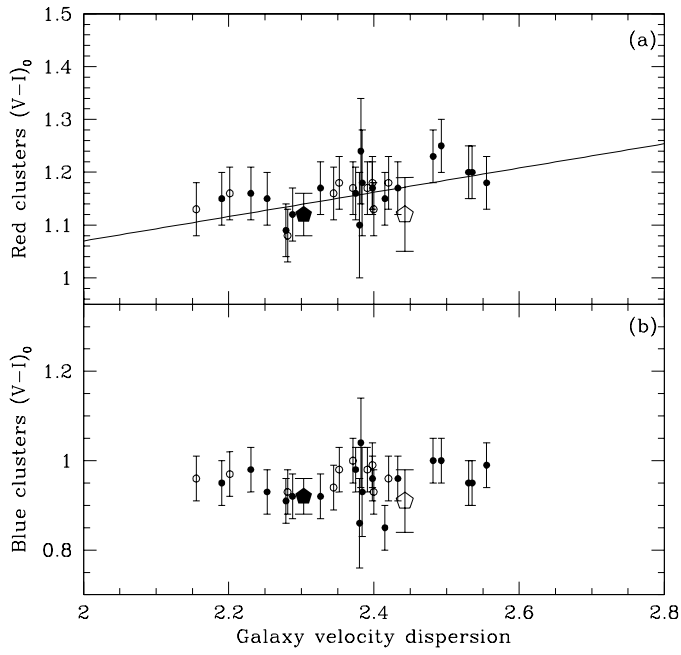


Figure 9.

Table 1. General properties of the observed galaxies.

	NGC 1199	NGC 6868
l	199.2	350.9
b	-57.3	-32.6
RA	03:03:38.6	20:09:54.1
DEC	-15:36:51	-48:22:47
Morph. Type	E2	E2
$B_T$	$12.5 \pm 0.13^a$	$11.4 \pm 0.11^b$
$M_V$	$-21.3 \pm 0.34$	$-21.9 \pm 0.29$
$(B - V)$	$0.99^b$	$1.00^b$
$V_{Rad}$	$2705 (km s^{-1})^b$	$2876 (km s^{-1})^b$
Distance	$33.1 (Mpc)^c$	$26.8 (Mpc)^c$
Effective Radius	$33.6''^d$	$38.4''^e$
Int. Vel. Disp.	$201 (km s^{-1})^f$	$277 (km s^{-1})^f$

<sup>a</sup>Hickson, Kindl and Auman (1989)

<sup>b</sup>Faber *et al.* (1989)

<sup>c</sup>Tonry *et al.* (2001)

<sup>d</sup>Zepf and Whitmore (1993)

<sup>e</sup>Kobayashi and Arimoto (1999)

<sup>f</sup>Prugniel and Simien (1996)

Table 2. Observational Information

Group	Band	Telesc.	Instr.	Date	Tot. Exp. [sec]	Pixel Size	# Ima.	Seeing ["]
HCG 22	B	Keck II	LRIS	06/02/1997	720	0.215	4	0.77
HCG 22	R	Keck II	LRIS	06/02/1997	630	0.215	7	0.74
NGC 6868 (1)	B	VLT	FORS1	10/10/1999	900	0.2	5	0.76
NGC 6868 (1)	R	VLT	FORS1	10/10/1999	810	0.2	9	0.73
NGC 6868 (2)	B	VLT	FORS1	10/11/1999	900	0.2	5	0.96
NGC 6868 (2)	R	VLT	FORS1	10/11/1999	810	0.2	9	0.89

Table 3. Detection completeness limit with the percentage of classification. Column (1) Image name, column (2) image band, column (3) completeness limit magnitude, column (4) percentage of detection at the completeness limit magnitude.

Image	band	Detec. Completeness	
		Mag. Limit	%
HCG 22	B	25.5	87.5
HCG 22	R	24.0	79.5
NGC 6868 (1)	B	24.5	90.2
NGC 6868 (1)	R	23.0	88.9
NGC 6868 (2)	B	24.5	88.3
NGC 6868 (2)	R	23.0	85.7

Table 4. Gaussian fit parameters. Column (1) image name, column (2) image band, column (3) peak position (fixed at  $M_V = -7.33$ ), column (4)  $\chi^2$  of the Gaussian fit, column (5) area of Gaussian covered by our data.

Image	Band	$m_0$	$\chi^2$	%
HCG 22	B	$26.2 \pm 0.3$	0.3214	$30.8 \pm 8.5$
HCG 22	R	$24.6 \pm 0.3$	0.2630	$33.4 \pm 8.7$
NGC 6868	B	$25.7 \pm 0.2$	0.2854	$18.7 \pm 5.3$
NGC 6868	R	$24.1 \pm 0.2$	0.1995	$20.9 \pm 5.2$

Table 5. Specific frequency values using the “core model” profile with the core radius ( $r_c$ ) proposed by Forbes *et al.* (1996) and a power-law profile. Column (1) estimative (Local values, core radius value in *kpc* for the “core model” profile and slope of the power-law profile, column (2) estimated number of globular clusters, column (3) estimated specific frequency.

	$N$	$S_n$
NGC 1199		
Local	$314 \pm 105$	$3.4 \pm 1.5$
$r_c = 2.19$	$1169 \pm 429$	$3.6 \pm 1.8$
$\alpha = 2.5 \pm 0.3$	$1668 \pm 899$	$5.2 \pm 3.2$
NGC 6868		
Local	$266 \pm 106$	$0.8 \pm 0.4$
$r_c = 2.58$	$1060 \pm 555$	$1.8 \pm 1.1$
$\alpha = 1.4 \pm 0.3$	$1089 \pm 503$	$1.9 \pm 1.0$